

Wigner time delay in photodetachmentSoumyajit Saha,^{1,*} Jobin Jose,^{2,†} Pranawa C. Deshmukh,^{3,4,‡} G. Aravind,^{1,§} Valeriy K. Dolmatov,^{5,||} Anatoli S. Kheifets,^{6,¶} and Steven T. Manson^{7,#}¹*Department of Physics, Indian Institute of Technology Madras, Chennai, Tamil Nadu 600036, India*²*Department of Physics, Indian Institute of Technology Patna, Bihta, Bihar 801013, India*³*Department of Physics, Indian Institute of Technology Tirupati, Tirupati, Andhra Pradesh 517506, India*⁴*Department of Physics, Indian Institute of Science Education and Research Tirupati, Tirupati, Andhra Pradesh 517507, India*⁵*Department of Physics and Earth Science, University of North Alabama, Florence, Alabama 35632, USA*⁶*Research School of Physics and Engineering, The Australian National University, Canberra ACT 0200, Australia*⁷*Department of Physics and Astronomy, Georgia State University, Atlanta, Georgia 30303, USA*

(Received 20 January 2019; published 8 April 2019)

Using Cl^- as a test case, Wigner time delay in the photodetachment process has been investigated theoretically, along with the photoionization of the isoelectronic Ar atom, for the outer $3p$ shell using the relativistic-random-phase approximation (RRPA). Time delay was probed in these systems from threshold to 80 eV, to investigate threshold effects, the centrifugal barrier shape resonance, and the Cooper minimum region. This study focuses on Cl^- because, for negative ions, the phase of the photoemission process is not dominated by the Coulomb phase as it is in photoionization. The results show significant differences, both qualitative and quantitative, between the time delays for Cl^- and Ar photoemission at low photoelectron energy, but they are rather similar in the Cooper minimum region, where the Coulomb phase is small. In particular, the Wigner time delay in Cl^- exhibits a dramatic energy dependence just above threshold, and a rapidly increasing time delay in the vicinity of the shape resonance. A strong angular dependence of time delay has also been found near the threshold region for the Cl^- case, and is absent in the case of the photoionization of Ar. The origin of these phenomenologies is explained and a prospectus for future work is presented.

DOI: [10.1103/PhysRevA.99.043407](https://doi.org/10.1103/PhysRevA.99.043407)**I. INTRODUCTION**

The motion of the electrons constituting atoms, molecules, and clusters is on the attosecond (as, 10^{-18} s) timescale [1]. One needs a very sophisticated and advanced theoretical methodology to accurately probe the ultrafast electronic motion and study this subatomic world. With the impetus of two pioneering experimental investigations [2,3], photoionization time delay studies, as a means of investigating attosecond phenomena, have gained quite a bit of attention in recent years; a selection of some of this work can be found in Refs. [4–18]. State-of-the-art experimental techniques have succeeded in probing the time domain in photoionization processes. The photoemission delay, measured using various pump-probe techniques, is an excellent way to investigate dynamical processes inside atoms. The measured time delay consists of two parts: (i) a Wigner time delay or WES (Wigner-Eisenbud-Smith) time delay (τ_W) [19–21], described as the energy derivative of the phase of the complex photoemission transition matrix element, and (ii) the delay resulting

from the interaction of the outgoing photoelectron with the laser field and the potential of the residual positive ion, known as Coulomb-laser-coupling delay (τ_{CLC}) [22] or continuum-continuum delay (τ_{CC}) [23]. Now, photodetachment is similar to the photoionization process, except that the ionizing electromagnetic pulse interacts with a negative ion, unlike the photoionization of an atom where the target is neutral [24]. In the photodetachment of a negative ion, a neutral atom is left behind so that the outgoing photoelectron does not experience a Coulomb potential in the asymptotic region, and the Coulomb part of the photoelectron phase is excluded from the total phase of the photoemission matrix element. Thus, since τ_{CC} (or τ_{CLC}) essentially vanishes, except very close to threshold, when the potential experienced by the escaping photoelectron is short range, as in photodetachment, the interpretation of photoemission time delay experiments is much more straightforward [25]. In addition, the Coulomb phase, which dominates the total phase near threshold in the case of photoionization, is absent for photodetachment, allowing the photoemission time delay studies in negative ions to efficiently probe the low-energy shape resonances and short-range interactions. Furthermore, unlike photoionization where the $l \rightarrow l + 1$ channels generally dominate the process at all energies except the Cooper minimum [26–28], in photodetachment the $l \rightarrow l - 1$ channels always dominate near threshold, owing to the Wigner threshold law [29]. Thus, the absence of the Coulomb phase allows for the study of the near-threshold and low-energy phenomena via time delay

*soumyajit147@gmail.com

†jobin.jose@iitp.ac.in

‡pcd@iitp.ac.in

§garavind@iitp.ac.in

||vkdolmatov@una.edu

¶a.kheifets@anu.edu.au

#smanson@gsu.edu

spectroscopy. The present work aims at the study of time delay in photoemission from a closed-shell negative ion and, for comparison, the isoelectronic Ar, with emphasis on the region of the centrifugal barrier shape resonances [26,30–32]. In our earlier study of photoionization time delay from noble gas neutral atoms [33], no significant effect of the shape resonance on the photoionization time delay was found. This was due to the large time delay near the threshold owing to the Coulomb phase, which overwhelmed the effect of the shape resonance. We have, therefore, undertaken time delay studies in the photodetachment of negative ions, since this process is free from the long-range Coulomb field effects in the final state. Preliminary results of the present studies were presented earlier [34,35]. Specifically, in the present work, we report the results of our study of the time delay in the photodetachment of Cl^- using the relativistic-random-phase approximation (RRPA) [36]. Also, for comparison, using the same methodology, we have investigated the time delay in the photoionization of the neutral atom which is, respectively, isoelectronic with the negative ion, i.e., Ar, in order to highlight time delay in the absence of a long-range Coulomb field in the final states of the photodetachment process. In addition, it has also been found that in the near-threshold region the time delay in the photodetachment process is angle sensitive and has a strong dependence on the angle of photoelectron ejection with respect to the direction of light polarization. On the other hand, the photoionization time delay does not exhibit any significant dependence on the angle of photoelectron ejection with respect to the direction of light polarization in this region. The RRPA is a relativistic many-body method that includes significant aspects of electron-electron correlations and, being fully relativistic (based on the Dirac equation), allows us to assess the importance of relativistic effects. The methodology and theory are presented in Sec. II. In Sec. III, we present and discuss our results. Conclusions are presented in Sec. IV.

II. THEORETICAL METHOD

The relativistic electric dipole amplitude, for a linearly polarized light along the z direction, for a transition from an initial state, $nljm$, to a final state, $\bar{\kappa}\bar{l}\bar{j}\bar{m}$, is given by [14]

$$[T^{1\nu}]_{nlj}^m = \sum_{\bar{\kappa}\bar{m}} C_{\bar{l}\bar{m}-\nu, 1/2\nu}^{\bar{j}\bar{m}} Y_{\bar{l}\bar{m}-\nu}(\hat{\kappa}) (-1)^{2\bar{j}+j+1-\bar{m}} \times \begin{pmatrix} \bar{j} & 1 & j \\ -\bar{m} & 0 & m \end{pmatrix} i^{1-\bar{l}} e^{i\delta_{\bar{\kappa}}} \langle \bar{a} | Q_1^{(1)} | a \rangle. \quad (1)$$

Here, $\bar{\kappa} = \mp(\bar{j} + \frac{1}{2})$ for $\bar{j} = (\bar{l} \pm \frac{1}{2})$, $\nu = \pm\frac{1}{2}$ is the photoelectron spin polarization, the C 's are the Clebsch-Gordon coefficients, the Y 's are the spherical harmonics, $\delta_{\bar{\kappa}}$ is the scattering phase, and an overall multiplicative factor has been ignored for simplicity. The reduced matrix element of the spherical tensor between the initial state $a = (n\kappa)$ and a final state $\bar{a} = (E, \bar{\kappa})$ is obtained from a solution of the RRPA equations [37] and, for simplification of the notation, we define

$$D_{n\kappa \rightarrow E\bar{\kappa}} = i^{1-\bar{l}} e^{i\delta_{\bar{\kappa}}} \langle \bar{a} | Q_J^{(\lambda)} | a \rangle \quad (2)$$

in terms of the reduced matrix element $\langle \bar{a} | Q_J^{(\lambda)} | a \rangle$ [37]. The expressions below show the relativistic ionization amplitudes

for np initial states,

$$\begin{aligned} [T^{1+}]_{np_{1/2}}^{m=\frac{1}{2}} &= +\frac{1}{\sqrt{15}} Y_{20} D_{np_{1/2} \rightarrow \epsilon d_{3/2}} + \frac{1}{\sqrt{6}} Y_{00} D_{np_{1/2} \rightarrow \epsilon s_{1/2}}, \\ [T^{1-}]_{np_{1/2}}^{m=\frac{1}{2}} &= -\frac{1}{\sqrt{10}} Y_{21} D_{np_{1/2} \rightarrow \epsilon d_{3/2}}, \\ [T^{1+}]_{np_{3/2}}^{m=1/2} &= \frac{1}{\sqrt{6}} Y_{00} D_{np_{3/2} \rightarrow \epsilon s_{1/2}} - \frac{1}{5\sqrt{6}} Y_{20} D_{np_{3/2} \rightarrow \epsilon d_{3/2}} \\ &\quad - \frac{1}{5} \sqrt{\frac{3}{2}} Y_{20} D_{np_{3/2} \rightarrow \epsilon d_{5/2}}, \\ [T^{1-}]_{np_{3/2}}^{m=1/2} &= \frac{1}{10} Y_{21} D_{np_{3/2} \rightarrow \epsilon d_{3/2}} - \frac{1}{5} Y_{21} D_{np_{3/2} \rightarrow \epsilon d_{5/2}}, \\ [T^{1+}]_{np_{3/2}}^{m=3/2} &= -\frac{3}{\sqrt{10}} Y_{21} D_{np_{3/2} \rightarrow \epsilon d_{3/2}} - \frac{2\sqrt{3}}{15} Y_{21} D_{np_{3/2} \rightarrow \epsilon d_{5/2}}, \\ [T^{1-}]_{np_{3/2}}^{m=3/2} &= \frac{\sqrt{3}}{5} Y_{22} D_{np_{3/2} \rightarrow \epsilon d_{3/2}} - \frac{\sqrt{3}}{15} Y_{22} D_{np_{3/2} \rightarrow \epsilon d_{5/2}}. \quad (3) \end{aligned}$$

Here, the amplitudes are expressed in terms of only positive m values. In the polarization axis direction \hat{z} , only the axial, Y_{00} , components of the spherical harmonics in Eq. (1) are nonzero, so only terms with $m = \nu = \pm\frac{1}{2}$ survive. Due to the axial symmetry, then, the final result does not depend on the sign of the spin and the angular momentum projections. The Wigner time delay associated with a particular transition ($n\kappa \rightarrow E\bar{\kappa}$) is [19–21]

$$\tau = \hbar \frac{d\eta_{\bar{\kappa}}}{dE}, \quad (4)$$

where $\eta_{\bar{\kappa}}$ is the energy-dependent phase of the photoemission complex matrix element,

$$\eta_{\bar{\kappa}} = \tan^{-1} \left[\frac{\text{Im} D_{n\kappa \rightarrow E\bar{\kappa}}}{\text{Re} D_{n\kappa \rightarrow E\bar{\kappa}}} \right]. \quad (5)$$

Similarly, the time delay for photoemission from a particular initial state is obtained using the same equations but with the transition amplitudes of Eq. (3), the T 's, instead of the D 's. Note that electron-ion scattering and photoionization processes are related through time-reversal symmetry [37], hence the above expression for photoemission time delay

TABLE I. Calculated and available experimental [39] thresholds.

Subshell (Cl^-)	DF (eV)	
$3p_{3/2}$	4.03	
$3p_{1/2}$	4.17	
$3s_{1/2}$	20.13	
$2p_{3/2}$	208.87	
$2p_{1/2}$	210.64	
$2s_{1/2}$	280.22	
Subshell (Ar)	DF (eV)	Expt. (eV)
$3p_{3/2}$	16.00	15.76
$3p_{1/2}$	16.19	15.95
$3s_{1/2}$	35.02	29.31
$2p_{3/2}$	259.78	
$2p_{1/2}$	262.07	
$2s_{1/2}$	337.73	

does not have the factor 2 found in the expressions of the Wigner time delay in a scattering formalism [19–21]. As mentioned above, the RRPA formulation [36] was employed in the present photodetachment and photoionization calculations. The RRPA method is gauge invariant and, aside from being explicitly relativistic, i.e., based on the Dirac equation, RRPA includes significant aspects of initial-state correlation, roughly equivalent to a very large configuration interaction calculation. In addition, RRPA includes correlation in the final continuum states in form of interchannel coupling among all of the relativistic single-ionization (single-excitation) channels. However, the RRPA is amenable to a further approximation which permits the use of selective interchannel coupling, known as the truncated RRPA, which can be employed to pinpoint the specific aspect(s) of interchannel coupling which are responsible for particular physical effects. The use of a truncated RRPA removes the gauge invariance; however, in

the present calculations, it is only at the few percent level, so it is not really an issue.

In addition, the threshold energies, the use of Dirac-Fock (DF) [38] energies, are required in the RRPA calculation to maintain gauge invariance. However, for comparison to experiments, it is useful to use experimental energies, where available, and our atomic calculations do just this. Although this destroys the exact equality of length and velocity gauges, here too the differences are only at the few percent level. The calculated DF energies, along with the available experimental energies [39] for comparison, are given in Table I, where it is seen that for the outer atomic subshells, the agreement is reasonably good.

Very few of the energy levels of negative ions are known experimentally, so they have been omitted from the table. However, for the halogen ion, Cl^- , the experimental electron affinity [40] of 3.61 eV compares reasonably well with the

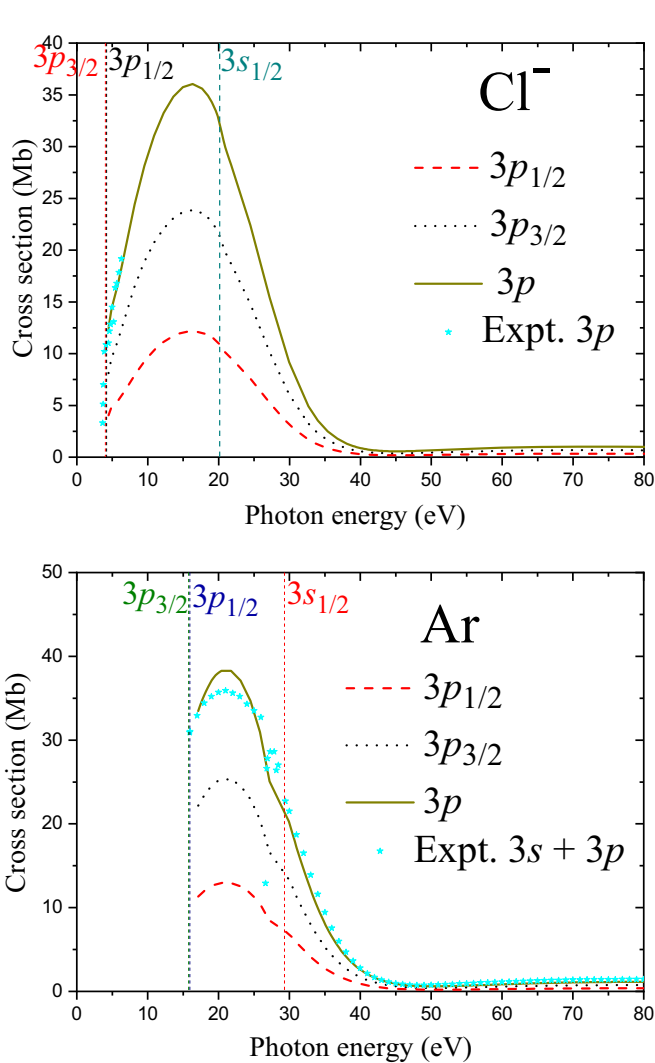


FIG. 1. Photoemission cross sections calculated for Cl^- (top panel) and Ar (bottom panel) showing $3p_{1/2}$ (dashed line), $3p_{3/2}$ (dotted line), and the sum, $3p$ (solid line), along with available experiments (solid asterisk): Cl^- [41,42], Ar [43]. Note that the Ar data are for the sum of $3s$ and $3p$ cross sections. Thresholds are indicated as vertical dashed lines.

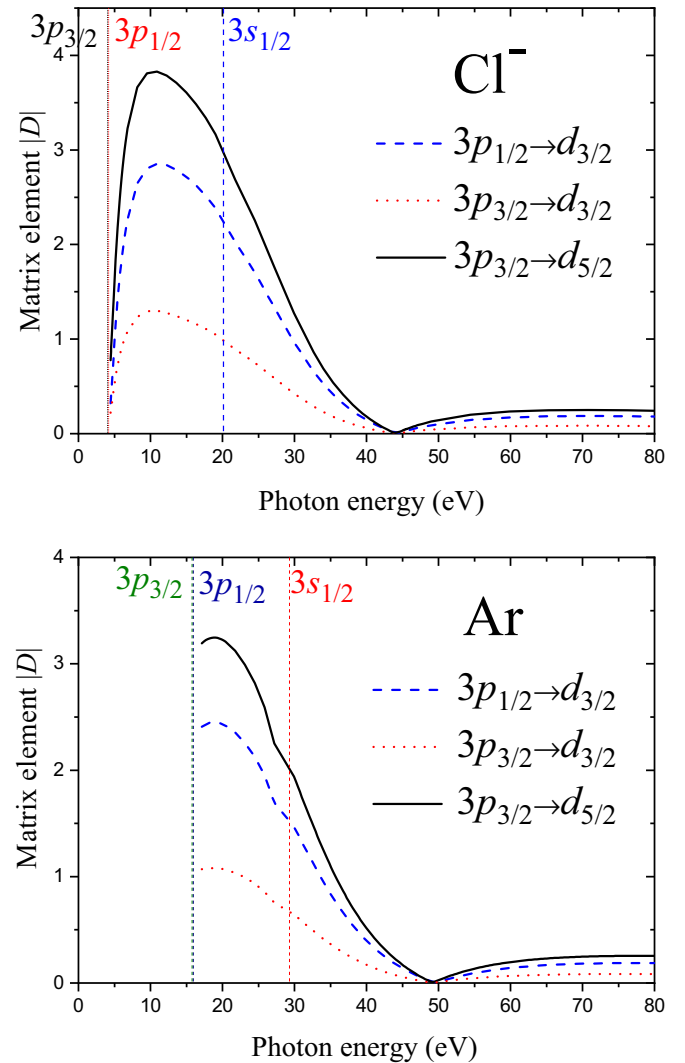


FIG. 2. The absolute values of the complex transition matrix elements $|D|$ as a function of photon energy for all the three relativistically split $3p \rightarrow d$ photoemission channels: $3p_{1/2} \rightarrow d_{3/2}$ (dashed line), $3p_{3/2} \rightarrow d_{3/2}$ (dotted line), and $3p_{3/2} \rightarrow d_{5/2}$ (solid line), in Cl^- (top panel) and Ar (bottom panel). Thresholds are indicated as vertical dashed lines.

theoretical outer-shell binding energy (Table I) of 4.03 eV, which indicates that the initial-state correlation is taken into account relatively well.

III. RESULTS AND DISCUSSION

The photoemission cross sections for Cl^- and Ar were calculated including all the relativistic dipole channels originating from $3p$, $3s$, $2p$, and $2s$, a total of 14 coupled channels, in each case; the $1s$ channels were omitted since they have essentially no effect in the photon energy ranges considered. The results are shown in Fig. 1, along with available experiments [41–43], which demonstrate excellent agreement with the calculations for both Cl^- and Ar. It is of importance to note that the cross sections for the negative ion and the atom are remarkably similar. The shape resonance (delayed maximum) is seen in both cases, along with the Cooper minimum [44] in the region of 40–50 eV photon energy. The only real difference between the two cases is near threshold where the atomic case exhibits a rather large cross section and varies slowly, as compared to the negative ion where

the photodetachment cross section vanishes at threshold, but increases very rapidly with energy. Figure 1 also shows that the $3p_{3/2}$ and $3p_{1/2}$ cross sections are of exactly the same shape and are in a ratio of 2:1, in both cases; this ratio simply reflects the occupation numbers of the two subshells. In other words, this suggests that relativistic effects are unimportant in both cases, in this region of the photoemission spectrum.

To explore this phenomenology further, the magnitudes (absolute values) of the matrix elements for all of the relativistic $3p \rightarrow d$ photoemission channels in Cl^- and Ar are presented in Fig. 2, where it is evident that the magnitudes of the matrix elements all have the same shape, in each case, as a function of energy. In addition, the $3p \rightarrow d$ shape resonances are clearly seen, as are the Cooper minima. The absolute values of the complex matrix elements reach their peak at a somewhat lower photon energy than the energy at which the cross section peaks, as one would expect since the cross section is scaled by the photon energy.

The phases of the complex matrix elements, along with the time delays derived from these phases using Eqs. (4) and (5), are shown in Fig. 3. Looking first at the phases, it is

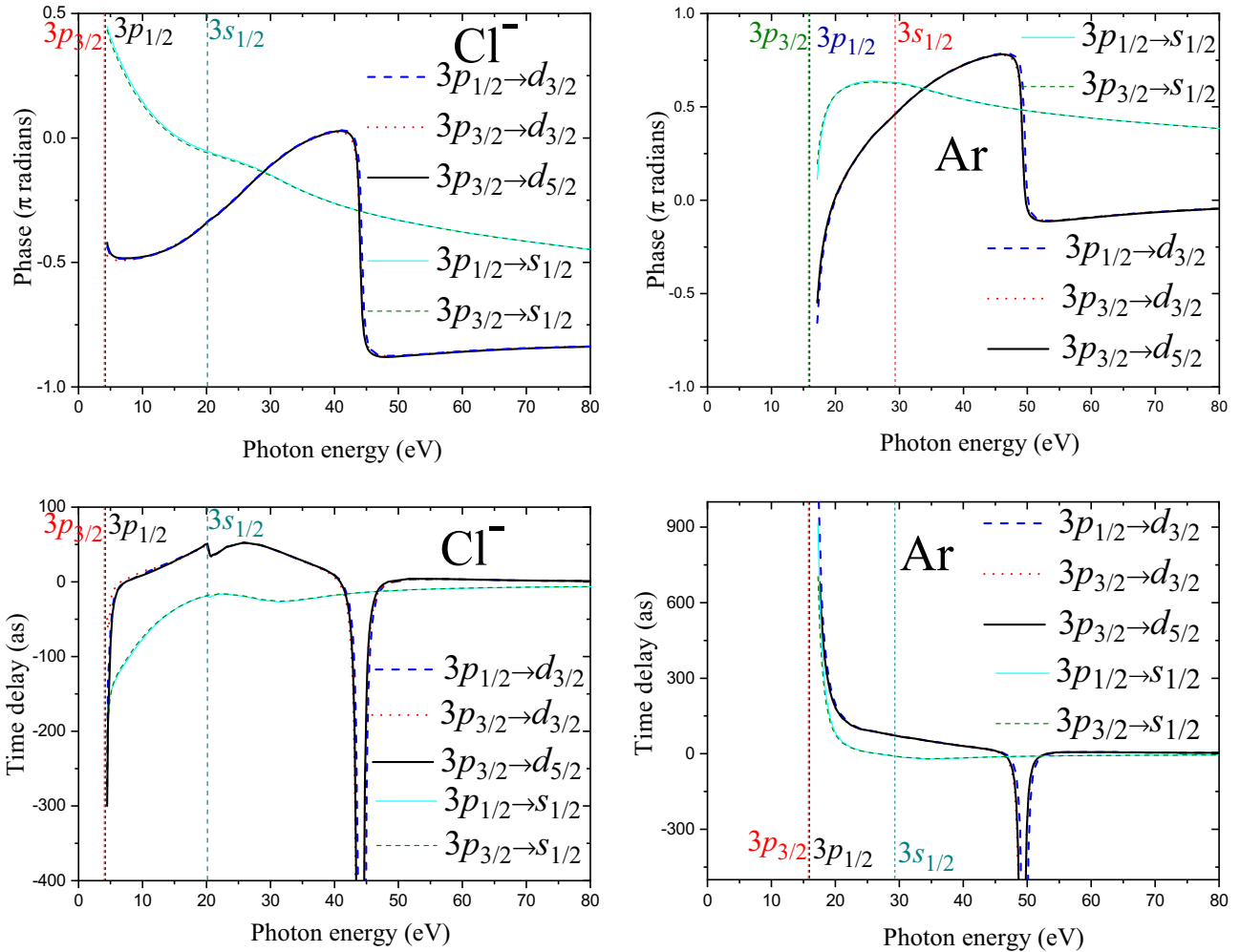


FIG. 3. Phases of the complex matrix elements for Cl^- (upper left) and Ar (upper right) as functions of energy for all five relativistic $3p$ photoemission channels: $3p_{1/2} \rightarrow d_{3/2}$ (thick dashed line), $3p_{3/2} \rightarrow d_{3/2}$ (thick dotted line), $3p_{3/2} \rightarrow d_{5/2}$ (thick solid line), $3p_{1/2} \rightarrow s_{1/2}$ (thin solid line), and $3p_{3/2} \rightarrow s_{1/2}$ (thin dashed line). The corresponding time delays are shown below each phase in attoseconds (as) (same line convention as in phase plot used). Thresholds are indicated as vertical dashed lines.

evident that, as expected from the cross sections, relativistic effects are rather unimportant as all of the $3p \rightarrow d$ phases lie essentially on top of one another, both for Cl^- and Ar, and the same is true for the $3p \rightarrow s$ phases. It is also clear that, above the $3s$ thresholds, the Cl^- and Ar phases are rather similar to each other with the $3p \rightarrow d$ phases displaying steep drops around the Cooper minima [33], and the $3p \rightarrow s$ phases decreasing monotonically [45], as expected. However, in the near-threshold region, the Cl^- and Ar phases are seen to be totally different. For Cl^- , the $3p \rightarrow d$ phases decrease slightly from threshold before showing a gradual increase reflecting the shape resonance; the $3p \rightarrow s$ phases are monotonically decreasing from threshold. For Ar, on the other hand, the phases are dominated by the Coulomb phases, in the near-threshold region, and these Coulomb phases (for all values of orbital angular momentum) go to infinity at threshold and drop rapidly with energy above threshold, leading to the observed behavior. Thus, the Coulomb phase contribution to the total phase obliterates any effects of the short-range atomic phase in the near-threshold region.

The time delays, for each of the cases, are also shown in Fig. 3. For Cl^- photodetachment the time delays are finite at threshold, quite negative (hundreds of attoseconds) and increasing, with the threshold values of the $3p \rightarrow d$ channels more negative than the $3p \rightarrow s$ but rising more rapidly owing to the $3p \rightarrow d$ shape resonance. Over the broad range to about 30 eV, the $3p \rightarrow d$ time delay is dominated by the shape resonance, although the effect of the Wigner cusp [29] in the $3p \rightarrow d$ channel is quite evident at the opening of the $3s$ detachment channel. This cusp is all but invisible in the phase, indicating that time delay spectroscopy might be useful in studying such cusp phenomena. At still higher energies, the time delay is dominated by the Cooper minimum behavior wherein the steep drop in the phase translates to a deep minimum in the time delay in the region of the Cooper minimum. In the Ar case, the time delay is positive infinity at threshold for both $3p \rightarrow d$ and $3p \rightarrow s$ transitions and rapidly increases with energy since the time delay is essentially due only to the Coulomb phase in this region.

It is quite evident that the effects of the $3p \rightarrow d$ shape resonance are almost completely masked by the Coulomb contribution, in the low-energy region. At the higher energies, the $3p \rightarrow d$ time delay is dominated by the Cooper minimum, just as in the Cl^- case. It is of interest to point out the possibility of measuring the time delays representing these individual matrix elements via spin-polarization spectroscopy [46].

One can also obtain the time delays for a particular initial state, as indicated above, using the phases of the amplitudes (T 's) of Eq. (3). Then, using Eqs. (4) and (5), the phases and time delays for photoemission from the $3p_{3/2}$ and $3p_{1/2}$ states of Cl^- and Ar are obtained. We concentrate first on Cl^- , where the results for the $3p_{3/2}$ and $3p_{1/2}$ states are almost identical, so only the phase for the $3p_{3/2}$ initial state has been shown in Fig. 4. This phase is similar to the results for the individual $3p \rightarrow d$ matrix elements of Fig. 3. This is because, over most of the energy range, the $3p \rightarrow d$ matrix element dominates the $3p \rightarrow s$. However, in the Cooper minimum region, the magnitude of the $3p \rightarrow d$ contribution to the amplitude diminishes (and nearly vanishes) so that the $3p \rightarrow s$

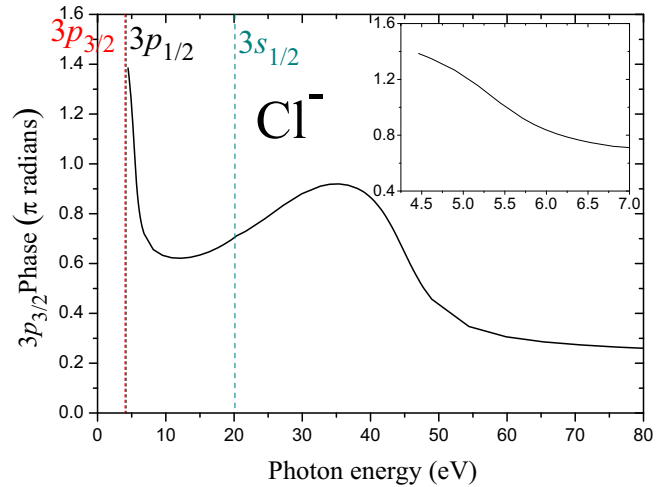


FIG. 4. Phase of the photodetachment amplitude for the $3p_{3/2}$ initial state of Cl^- in the direction of the photon polarization. The inset shows a closeup of the threshold region.

contribution to the amplitude, in Eq. (3), becomes much more important. Of greater significance, at the threshold of a photodetachment process, the transition to the lower angular momentum final state, in this case the $3p \rightarrow s$ transitions, always dominates, as embodied in the Wigner threshold law [29]. Thus, close to threshold, the $3p \rightarrow s$ matrix element dominates, but rather quickly, in a few eV, the $3p \rightarrow d$ matrix becomes larger. The phase near threshold, as seen in the inset in Fig. 4, exhibits a slope at threshold characteristic of the $3p \rightarrow s$ transition which changes to the slope related to the $3p \rightarrow d$ transition.

These changes in slope engender important changes in the Wigner time delay in the near-threshold region, as seen in Fig. 5 where a huge dip is exhibited, just above threshold, which is simply a result of the changeover in dominance of the $3p \rightarrow d$ and $3p \rightarrow s$ matrix elements as a function of energy; actually, it is the average $3p$ time delay shown in

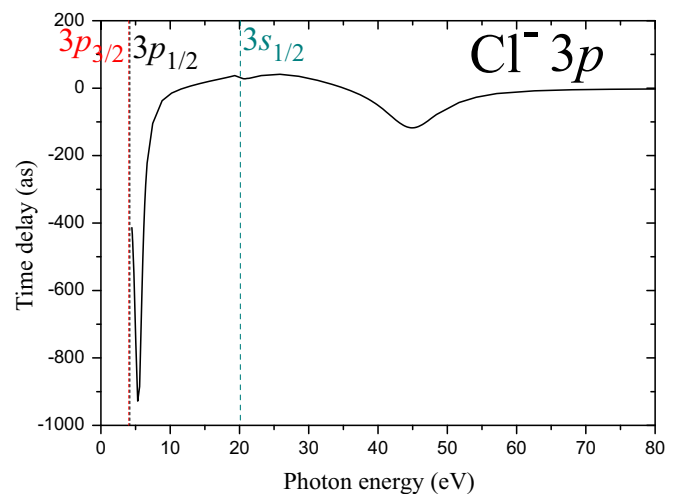


FIG. 5. Wigner time delay for the photodetachment of the $3p$ state of Cl^- , averaged over the $3p_{1/2}$ and $3p_{3/2}$ states.

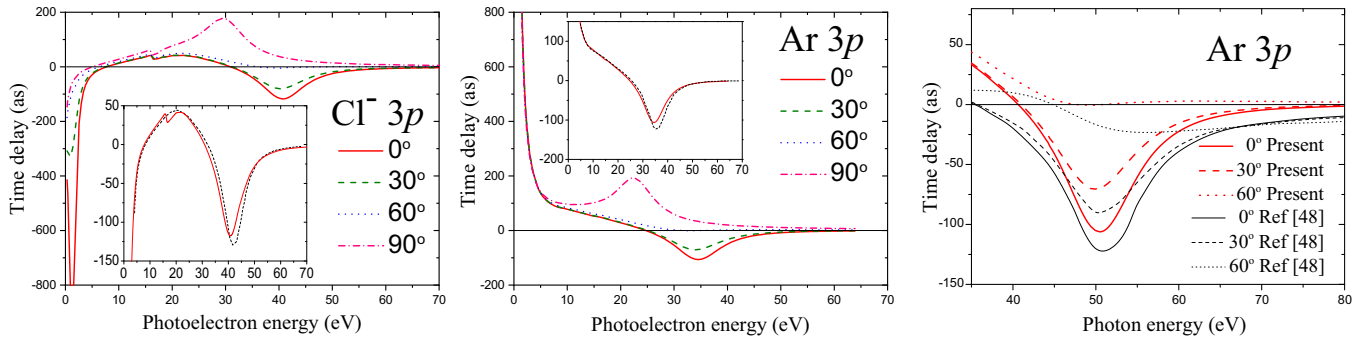


FIG. 6. Wigner time delay in the photodetachment of the $3p$ state of Cl^- (left panel) and in the photoionization of the $3p$ state of Ar (central and right panels), averaged over the $3p_{1/2}$ and $3p_{3/2}$ states shown for different photoelectron ejection angles (0° : solid line; 30° : dashed line; 60° : dotted line; 90° : dashed-dotted line,) with respect to the direction of polarization. In the first two panels the time delay evaluated only in the direction of polarization (0° angle) has been shown in the inset on a different scale for the $3p$ states of Cl^- and Ar, respectively; present results (solid line), Ref. [25] (dashed line). In the right panel a comparison with the angular-resolved atomic time delay of Ar $3p$ from Ref. [48] is shown in the region of the Cooper minimum.

Fig. 5; this is simply the sum of the $3p_j$ time delays weighted by the ratios of the respective differential cross sections in the polarization direction to the sum of the cross sections. But, since relativistic effects are so small here, this is also the Wigner time delay for photoemission from the $3p_{3/2}$ and $3p_{1/2}$ initial states individually. In addition, owing to the contribution of the $3p \rightarrow s$ matrix element in the region of the $3p \rightarrow d$ Cooper minimum, the very narrow and deep minima in the $3p \rightarrow d$ time delay, shown in Fig. 3, are seen to be much wider and shallower. It is of importance to note that the near-threshold structure is likely a general feature of Wigner time delay in the photodetachment of negative ions for all the nl subshells, inner and outer, for $l \neq 0$, owing to the Wigner threshold law since the $l \rightarrow l - 1$ partial wave always dominates at threshold, and the $l \rightarrow l + 1$ generally dominates at the higher energies.

These averaged results for Wigner time delay for both Cl^- and Ar are shown in Fig. 6 for different ejection angles relative to the direction of light polarization. The Cl^- results for 0° are the same as shown in Fig. 5, but on a different scale. The time delay spectra for 0° angle have been shown separately for both Cl^- and Ar in inset in their respective panel. The Ar time delay is similar to the time delays of the individual $3p \rightarrow d$ matrix elements in Fig. 3, except for the Cooper minimum region where, as was the case for Cl^- , the $3p \rightarrow s$ term in the amplitude, Eq. (3), moderates the effects, making the dip in that region wider and shallower as seen in the inset in the central panel. Also shown in the insets of Fig. 6 are the results of the calculation of Ref. [25] in which a rather different calculational methodology is used. The fact that there is good agreement, for both Cl^- and Ar, rather validates both calculations. This is of particular importance for the Cl^- case because correlation in both initial and final states is crucial to the accuracy of negative-ion photodetachment calculations. It should also be mentioned that another recent calculation on Ar, based upon the time-dependent local-density approximation (TDLDA), gives substantially the same results as presented in Fig. 6 [47]. A comparison has also been shown between the present results for Ar and the results presented in Ref. [48], though the time delay that has been shown in Ref. [48] is the total atomic

delay. Now the most important thing to notice in Fig. 6 is the strong angular dependence of the photodetachment time delay in the near-threshold region (left panel). However, there is no angular dependence of the time delay for the case of photoionization of Ar in the near-threshold region as seen in the central panel. It is also noticeable for the Cl^- case that the dip near threshold is prominent only in the case of the 0° angle and it was diminished with increasing angles. We can say that for higher angles the $3p \rightarrow s$ transition dominates only in close proximity to the threshold region and the $3p \rightarrow d$ transition overtakes $3p \rightarrow s$ even very near to the threshold.

IV. CONCLUSION

The Wigner time delay for the photodetachment of the negative ion Cl^- has been studied in detail, along with the photoionization of the isoelectronic Ar atom for comparison. The absence of a Coulomb tail in the potential “seen” by the photoelectron in the photodetachment process results in the time delay for Cl^- being rather different from Ar at low photoelectron energies, since the contribution of the Coulomb phase overwhelms the short-range phase for Ar. In contrast, the short-range contribution is the only constituent of the phase in the low-energy photoemission for Cl^- . Thus, the photodetachment time delay is sensitive to correlation and shape resonances at low photoelectron energies, while photoionization time delay is not. The calculated results confirm this viewpoint and the low-energy photodetachment time delay is seen to be very different from the photoionization time delay over the first 20 eV or so of photoelectron energy. Not only are the effects of the $p \rightarrow d$ shape resonance seen for Cl^- , but also a huge near-threshold variation with energy owing to the change in dominance of the $3p \rightarrow s$ transition at threshold to the $3p \rightarrow d$ transition a few eV above threshold. A similar strong variation of the time delay is seen in respect to the photoelectron emission direction. Both variations are a consequence of the Wigner threshold law for photodetachment [29]. Since the Wigner law applies to the photodetachment of all non- s states of all negative ions, i.e., there is nothing special about Cl^- , the rich structure in the time delay just above threshold is likely to be present in

most if not in all cases, i.e., this is expected to be a very general phenomenon. Thus, time delay spectroscopy could prove to provide significant insight into the near-threshold photodetachment process in addition to the study of low-energy shape resonances. In the near-threshold region the strong angular dependence of photodetachment time delay was also found. However, this is completely absent for the case of photoionization of Ar.

It was also seen that, although the effects of the Wigner cusp, which occurs at an inner $3s$ threshold for Cl^- , is hidden in the phase, it is evident in the time delay, thereby indicating that time delay spectroscopy might be useful in the investigation of these Wigner cusps. It is further demonstrated that, in the vicinity of the Cooper minima, there are rapid changes in the phases and deep dips in the time delays for both Cl^- and Ar; this is because the Coulomb phase is quite small in the energy region of the Cooper minimum in Ar, so the short-range phase dominates here. Furthermore, although the present calculations are explicitly relativistic (based upon the Dirac equation), it is found that relativistic interactions play essentially no part in the Wigner time delay for outer-shell photoemission at such low Z . However, it is likely that this

will not be the case for higher Z , since relativistic effects generally become more important for heavier atoms. To probe the conditions under which relativistic interactions are important in the Wigner time delay for photodetachment, a series of calculations for heavier systems is in progress; included in this investigation is the photodetachment of nd and nf subshells in an effort to ascertain how the insights obtained from np subshells apply to higher angular momentum states.

ACKNOWLEDGMENTS

This work was supported by the infrastructure and hospitality provided by the Director, IIT Tirupati. S.S. is thankful to IIT Patna for the hospitality and support he received during his visit to IIT Patna to do one part of the work. J.J. acknowledges the support provided by SERB through Project No. ECR/2016/001564. S.T.M. acknowledges the support provided by the Chemical Sciences, Geosciences, and Biosciences Division, Office of Basic Energy Sciences, Office of Science, U.S. Department of Energy, Grant No. DE-FG02-03ER15428.

-
- [1] P. B. Corkum and F. Krausz, *Nat. Phys.* **3**, 381 (2007).
- [2] M. Schultze, M. Fieß, N. Karpowicz, J. Gagnon, M. Korbman, M. Hofstetter, S. Neppl, A. L. Cavalieri, Y. Komninos, T. Mercouris, C. A. Nicolaides, R. Pazourek, S. Nagele, J. Feist, J. Burgdörfer, A. M. Azzeer, R. Ernstorfer, R. Kienberger, U. Kleineberg, E. Goulielmakis, F. Krausz, and V. S. Yakovlev, *Science* **328**, 1658 (2010).
- [3] K. Klünder, J. M. Dahlström, M. Gisselbrecht, T. Fordell, M. Swoboda, D. Guénot, P. Johnsson, J. Caillat, J. Mauritsson, A. Maquet, R. Taïeb, and A. L'Huillier, *Phys. Rev. Lett.* **106**, 143002 (2011).
- [4] R. Pazourek, S. Nagele, and J. Burgdörfer, *Rev. Mod. Phys.* **87**, 765 (2015), and references therein.
- [5] A. S. Kheifets, S. Saha, P. C. Deshmukh, D. A. Keating, and S. T. Manson, *Phys. Rev. A* **92**, 063422 (2015).
- [6] M. Sabbar, S. Heuser, R. Boge, M. Lucchini, T. Carette, E. Lindroth, L. Gallmann, C. Cirelli, and U. Keller, *Phys. Rev. Lett.* **115**, 133001 (2015).
- [7] M. Kotur, D. Guénot, Á. Jiménez-Galán, D. Kroon, E. W. Larsen, M. Louisy, S. Bengtsson, M. Miranda, J. Mauritsson, C. L. Arnold, and S. E. Canton, *Nat. Commun.* **7**, 10566 (2016).
- [8] P. Hockett, E. Frumker, D. M. Villeneuve, and P. B. Corkum, *J. Phys. B* **49**, 095602 (2016).
- [9] M. Huppert, I. Jordan, D. Baykusheva, A. von Conta, and H. J. Wörner, *Phys. Rev. Lett.* **117**, 093001 (2016).
- [10] S. Heuser, Á. Jiménez Galán, C. Cirelli, C. Marante, M. Sabbar, R. Boge, M. Lucchini, L. Gallmann, I. Ivanov, A. S. Kheifets, J. M. Dahlström, E. Lindroth, L. Argenti, F. Martín, and U. Keller, *Phys. Rev. A* **94**, 063409 (2016).
- [11] D. A. Keating, P. C. Deshmukh, and S. T. Manson, *J. Phys. B* **50**, 175001 (2017).
- [12] L. Gallmann, I. Jordan, H. J. Wörner, L. Castiglioni, M. Hengsberger, J. Osterwalder, C. A. Arrell, M. Chergui, E. Liberatore, U. Rothlisberger, and U. Keller, *Struct. Dynam.* **4**, 061502 (2017).
- [13] C. A. Nicolaides, *Appl. Sci.* **8**, 533 (2018).
- [14] D. A. Keating, S. T. Manson, V. K. Dolmatov, A. Mandal, P. C. Deshmukh, F. Naseem, and A. S. Kheifets, *Phys. Rev. A* **98**, 013420 (2018).
- [15] P. C. Deshmukh, A. Kumar, H. R. Varma, S. Banerjee, S. T. Manson, V. K. Dolmatov, and A. S. Kheifets, *J. Phys. B* **51**, 065008 (2018).
- [16] C. Cirelli, C. Marante, S. Heuser, C. L. M. Petersson, Á. J. Galán, L. Argenti, S. Zhong, D. Busto, M. Isinger, S. Nandi, S. Maclot, L. Rading, P. Johnsson, M. Gisselbrecht, M. Lucchini, L. Gallmann, J. M. Dahlström, E. Lindroth, A. L'Huillier, F. Martín, and U. Keller, *Nat. Commun.* **9**, 955 (2018).
- [17] A. W. Bray, F. Naseem, and A. S. Kheifets, *Phys. Rev. A* **97**, 063404 (2018).
- [18] M. Ossiander, J. Riemensberger, S. Neppl, M. Mittermair, M. Schäffer, A. Duensing, M. S. Wagner, R. Heider, M. Wurzer, M. Gerl, M. Schnitzenbaumer, J. V. Barth, F. Libisch, C. Lemell, J. Burgdörfer, P. Feulner, and R. Kienberger, *Nature (London)* **561**, 374 (2018).
- [19] E. P. Wigner, *Phys. Rev.* **98**, 145 (1955).
- [20] L. Eisenbud, Ph.D. thesis, Princeton University, 1948.
- [21] F. T. Smith, *Phys. Rev.* **118**, 349 (1960).
- [22] R. Pazourek, S. Nagele, and J. Burgdörfer, *Faraday Discuss.* **163**, 353 (2013).
- [23] J. M. Dahlström, A. L'Huillier, and A. Maquet, *J. Phys. B* **45**, 183001 (2012).
- [24] V. K. Ivanov, *Radiat. Phys. Chem.* **70**, 345 (2004), and references therein.
- [25] E. Lindroth and J. M. Dahlström, *Phys. Rev. A* **96**, 013420 (2017).
- [26] U. Fano and J. W. Cooper, *Rev. Mod. Phys.* **40**, 441 (1968).

- [27] A. F. Starace, in *Handbuch der Physik*, edited by W. Mehlhorn (Springer, Berlin, 1982), Vol. 31, pp. 1–121.
- [28] S. T. Manson, *Adv. Electron. Electron Phys.* **41**, 73 (1976); **44**, 1 (1978).
- [29] E. P. Wigner, *Phys. Rev.* **73**, 1002 (1948).
- [30] S. T. Manson and J. W. Cooper, *Phys. Rev.* **165**, 126 (1968).
- [31] A. R. P. Rau and U. Fano, *Phys. Rev.* **167**, 7 (1968).
- [32] J. P. Connerade, *Highly Excited Atoms* (Cambridge University Press, London, 1998).
- [33] S. Saha, A. Mandal, J. Jose, H. R. Varma, P. C. Deshmukh, A. S. Kheifets, V. K. Dolmatov, and S. T. Manson, *Phys. Rev. A* **90**, 053406 (2014).
- [34] S. Saha, P. C. Deshmukh, J. Jose, A. S. Kheifets, and S. T. Manson, *Bull. Am. Phys. Soc.* **61**, 53 (2016).
- [35] S. Saha, J. Jose, P. C. Deshmukh, A. S. Kheifets, V. K. Dolmatov, and S. T. Manson, *Bull. Am. Phys. Soc.* **62**, 206 (2017).
- [36] W. R. Johnson and C. D. Lin, *Phys. Rev. A* **20**, 964 (1979).
- [37] P. C. Deshmukh, D. Angom, and A. Banik, *Atomic and Molecular Physics DST-SERC School* (Narosa, New Delhi, 2012).
- [38] I. P. Grant, *Relativistic Quantum Theory of Atoms and Molecules*, Springer Series on Atomic, Optical and Plasma Physics (Springer, New York, 2007).
- [39] Y. Ralchenko, A. E. Kramida, J. Reader, and NIST ASD Team, *NIST Atomic Spectra Database (version 3.1.5)*, Technical Report (National Institute of Standards and Technology, Gaithersburg, MD, 2011), <http://physics.nist.gov/asd>.
- [40] T. Andersen, H. K. Haugen, and H. Hotop, *J. Phys. Chem. Ref. Data* **28**, 1511 (1999).
- [41] A. Mandl, *Phys. Rev. A* **14**, 345 (1976).
- [42] V. Radojević, H. P. Kelly, and W. R. Johnson, *Phys. Rev. A* **35**, 2117 (1987).
- [43] J. Samson and W. Stolte, *J. Electron Spectrosc. Relat. Phenom.* **123**, 265 (2002).
- [44] J. W. Cooper, *Phys. Rev.* **128**, 681 (1962).
- [45] S. T. Manson, *Phys. Rev.* **182**, 97 (1969).
- [46] M. Fanciulli, H. Volfová, S. Muff, J. Braun, H. Ebert, J. Minár, U. Heinzmann, and J. H. Dil, *Phys. Rev. Lett.* **118**, 067402 (2017).
- [47] L.-W. Pi and A. S. Landsman, *Appl. Sci.* **8**, 00322 (2018).
- [48] J. M. Dahlström and E. Lindroth, *J. Phys. B* **49**, 209501 (2016).